New Developments in Superconductivity Research (ed. R.W. Stevens, Nova Science, New York, 2003), pp. 101-129

On Critical Current Enhancement in Dislocated, Deoxygenated and Particle Irradiated Superconductors: A Unified Approach

Sergei Sergeenkov

March 29, 2005

Bogoliubov Laboratory of Theoretical Physics,
Joint Institute for Nuclear Research, 141980 Dubna, Russia

1 Introduction

As is well-known [1], the technological usage of any superconducting materials is based on their ability to carry (without loss) significant critical currents in strong enough applied magnetic fields. This ability is directly related to pinning efficiency of a given material which in turn is determined by its crystallographic structure and the presence of different kinds of defects (both inherent and introduced artificially). In conventional superconductors, the magnetic flux flowing through the crystal is assumed to be pinned by practically *immobile* (frozen) pinning centers (except perhaps for a possibility of thermal fluctuations around their equilibrium positions). In high-T_c superconductors (HTS) the situation is much more complicated because of the smallness of their coherence length and, as a result, of practically inevitable formation of intricate weak-link structure even within a single grain (the so-called intragranular granularity [2]). Hence, any defects (imperfections) in these materials will contribute not only to their flux pinning ability but will also determine their weak-link properties. Such dualism brings about a lot of interesting anomalies in HTS (for the recent reviews on the subject, see, e.g., [3, 4] and further references therein) and calls for non-traditional pinning scenarios capable of explaining the observed non-trivial electronic transport behavior in these materials. In the present paper, one of the possible scenarios is proposed based on a novel concept of vortex pinning via defect-induced intragrain weak links which takes advantage of the above-mentioned dualism of (extended) defects (as pinning centers and weak links) in HTS by allowing pinning centers to participate in the pinning process more actively. By considering a subtle balance between different forces acting upon an extended (dislocations) and point (oxygen vacancies) defects to stabilize their

equilibrium position inside a crystal, the scenario allows us to introduce external fields which control the defect behavior of the superconducting sample and, as a result, enables to describe (at least qualitatively) a rather wide set of the observed anomalous properties of HTS crystals (see Section 2). The paper is organized as follows. In Section 2 we review some of the key experimental results which will be discussed within the proposed scenario (outlined in Section 3) in the next sections. In Section 4 we consider pinning force improvement in screw dislocated thin films (and related electric field induced phenomena). Section 5 deals with the so-called fishtail anomaly (or peak effect) in oxygen-depleted single crystals and stoichiometric melt-textured materials. In Section 6 we demonstrate a substantial critical current density enhancement in particle irradiated crystals. And finally, in Section 7 we summarize the obtained results and discuss the important consequences of the proposed here unified scenario for optimization of some application oriented vital characteristics of high-T_c superconductors.

2 Review of the key experimental results

Recall [5] that there are serious arguments to consider the twinning boundary (TB) in HTS as insulating regions of the Josephson SIS-type structure. In particular, intragranular weak links due to the structural defects have been discussed by Schnelle et al. [6] and Hervieu et al. [7]. They observed antiphase boundaries, twinning, and "tilt" boundaries, and considered structural models for these different boundaries as well as their influences upon HTS properties. Additional evidence in favor of this conclusion is due to observed deviations in stoichiometry at the TB. As was shown by Zhu et al. [8] for $YBa_2(Cu_{1-x}M_x)_3O_{7-\delta}$ samples, the TB thickness is changed from $7\dot{A}$ (for $M = Ni, x = 0.02$, and $\delta = 0$) to $26\dot{A}$ (for $M = Al, x = 0.02$, and $\delta = 0$), while for a pure $YBa_2Cu_3O_7$ it gives $\simeq 10\dot{A}$. If after Zhu et al. [9] we assume that the physical thickness of the TB is of the order of an interplane distance (atomic scale), then such a boundary should rather rapidly move via the movement of the twinning dislocations. And this type of motion indeed has been observed by the electron-microscopic images in HTS [10, 11, 12]. As a result of the structural phase transition (if special precautions have not been done) a HTS sample is divided into a large number of twinning blocks [13], i.e. the sample is crossed by a large number of insulating layers (twin boundaries). An average distance between boundaries is essentially less than the grain size. This net of layers induces the net of Josephson junctions inside a single grain. In addition, the well known processes of the oxygen ordering in HTS leads to the continuous change of the lattice period along TB with the change of the oxygen content [14, 15]. Babcock and Larbalestier [16] observed the regular networks of localized grain boundary dislocations (GBDs) with the spacing ranged from $10nm$ to $100nm$. They concluded that closely spaced GBDs may produce effectively continuous normal or insulating barriers at the boundary which then behave like a planar SNS or SIS junction. Cai et al. [17] observed pronounced

peaks in the critical-current density in $YBa_2Cu_3O_7$ bicrystals well above the lower critical field. These peaks correspond to the fields for which the spacing between intragrain vortices is commensurate with the wavelength of the periodic grain boundary facet structure observed in the same bicrystals. In turn, Tsu et al. [18] made an important comparison of grain boundary topography and dislocation network structure in bulk-scale [001] tilt bicrystals of $Bi_2Sr_2CaCu_2O_8$ and $YBa_2Cu_3O_7$. At the same time, Diaz et al. [19] and Shang et al. [20] found clear evidence for vortex pinning by dislocations in $YBa_2Cu_3O_7$ low-angle grain boundaries and observed dislocations inside the grains along with coherent intragranular boundaries acting as weak links. By imaging epitaxial $YBa_2Cu_3O_{7-\delta}$ films with scanning tunneling microscopy, Gerber et al. [21] have directly observed screw dislocations with densities of $\simeq 10^9 cm^{-2}$ sufficient to account for a major part of the pinning forces and for weak links contribution in their films. Chen et al. [22] found the strong correlation between high density of the TBs and critical current density enhancement in $YBa_2Cu_3O_{7-\delta}$ films. A more direct evidence as for influence of dislocations on the pinning ability of HTS has been obtained by Mannhart et al. [23] (and recently confirmed by Hlubina et al. [24]) in screw dislocated HTS single crystals. They detected a nearly linear increase of the critical current density with the number of dislocations as well as a substantial improvement of $j_c(H)$ in applied magnetic field (at least, up to $0.05T$). The use of the same screw dislocated thin films in the so-called superconducting field-effect transistor (SuFET) devices allowed Mannhart et al. [25] to detect the electric-field induced modulation of critical current density in their films. Depending on the gate polarity, a quite tangible change (increase or decrease) of $j_c(E)$ has been observed.

Recent STM-based imaging of the granular structure in underdoped crystals of $Bi_2Sr_2CaCu_2O_{8+\delta}$ [26] revealed an apparent segregation of its electronic structure into superconducting domains (of the order of a few nanometers) located in an electronically distinct background. In particular, it was found that at low levels of hole doping ($\delta < 0.2$), the holes become concentrated at certain hole-rich domains. Tunneling between such domains leads to intrinsic granular superconductivity (GS) in HTS. Probably one of the first examples of GS was observed in $YBa_2Cu_3O_{7-\delta}$ single crystals in the form of the so-called fishtail anomaly of magnetization [27, 28, 29, 30]. In particular, Yang et al. [27] found out that dislocation networks provide effective pinning centers when the characteristic length scale of network matches that of the vortex spacing. They stressed that in high-T_c superconductors, oxygen vacancies are effective flux-pinning centers at low temperatures while the high temperature spatial variation of the oxygen ordering may well account for the anomalous fishtail magnetization feature in $YBa_2Cu_3O_{7-\delta}$ crystals. Daeumling et al. [28] discussed a rather intriguing correlation between defect pinning, intragrain weak links, and oxygen deficiency in $YBa_2Cu_3O_{7-\delta}$ single crystals. In particular, they have found that as the nominal oxygen deficiency δ decreases towards zero, the flux pinning declines and the crystals lose their explicitly granular signature. The above anomalous magnetic-field behavior has been attributed to the field-induced intragrain granularity in oxygen-depleted materials [29]. A phase

diagram $H_m(\delta, T)$ that demarcates the multigrain onset as a function of temperature and oxygen deficiency reconstructed by Osofsky et al. [30] allowed them to confirm that their single crystals exhibited behavior characteristic of homogeneous superconductors for $H < H_m$ and inhomogeneous superconductors for $H > H_m$. The granular behavior for $H > H_m$ has been related to the clusters of oxygen defects (within the CuO plane) that restrict supercurrent flow and allow excess flux to enter the crystal. The field at which the fishtail anomaly occurs was found [31, 32, 33] to decrease both with increasing the temperature and oxygen deficiency. This in turn suggests that the characteristic scale of the defect network structure is strongly dependent on oxygen stoichiometry. On the other hand, Ullrich et al. [34, 35] have observed a rather substantial critical current enhancement in stoichiometric melt-textured crystallites with the dislocation density of $\cong 2 \times 10^{10} cm^{-2}$. They argue that the strained region surrounding a dislocation can cause the fishtail anomaly as well. Indeed, since the strained regions near the dislocation core as well as oxygen-deficient regions are both result in a lower B_{c2} (the upper critical field) compared to the $YBa_2Cu_3O_{7-\delta}$ matrix, they become (normal conducting) pinning centers if the external magnetic field exceeds their upper critical field. The microstructure of subgrain boundaries occurring in single-domain $RBa_2Cu_3O_7$ ($R = Y$ and Nd) melt-textured composites has been studied by Sandiumenge et al. [36] using transmission electron microscopy. It was found that subgrain boundaries (SGB's) have a strong tendency to develop parallel to the (100), (010), and (110) planes, while the form of dislocation networks is controlled by the properties of constituting dislocations. Besides the underlying dislocation networks, SGB's may develop mesostructures such as faceting and stepped interfaces accommodating the deviation from low-index planes. The scaling and relaxation behavior around the fishtail minimum was studied in detail by Jirsa et al. [37] in a wide temperature range on $DyBa_2Cu_3O_7$ single crystals exhibiting a pronounced fishtail effect. It is also important to mention a recent paper of Banerjee et al. [38] who investigated evolution of the peak effect with defect structure in $YBa_2Cu_3O_7$ thin films at microwave frequencies.

Another important way to improve pinning ability of HTS single crystals is to use irradiation to incorporate (in a controllable way) different types of defects into these materials. Civale et al. [39, 40] achieved the pinning enhancement at high fields and high temperature for vortex confinement by columnar defects in $YBa_2Cu_3O_{7-\delta}$ crystals. Aligned columns of damaged material $50\dot{A}$ in diameter and $15\mu m$ long were produced by $580 Mev\ Sn$ ion irradiation. The pinning obtained was much greater than that produced by random point defects, and caused a considerable enlargement of the irreversibility region in the $H - T$ plane. Hardy et al. [41, 42] have measured magnetic properties of the Pb ion irradiated $YBa_2Cu_3O_{7-\delta}$ crystals and found a rather strong fluence dependence of irradiation-induced critical current enhancement $j_c(\Phi, H)$. The maximum of $j_c(\Phi, H)$ was found to shift to higher fluences with increasing the applied field and to higher fields with increasing the irradiation fluence. An important correlation between the extent of radiation damage and the oxygen stoichiometry of the sample has been observed by Zhu et al. [43]. They found that decrease

of δ significantly reduces the radiation damage. More evidence in favor of this conclusion has been provided by Li et al. [44]. They observed a self-doping caused by oxygen displacements in heavy-ion-irradiated $Bi_2Sr_2CaCu_2O_8$ crystals. Specially designed heavy-ion irradiation experiments have been carried out for single crystals of $YBa_2Cu_4O_8$ by Ming Xu et al. [45] in order to compare the magnetic-field dependence of the flux pinning for damage channels with the intrinsic fishtail pinning that occurs in this material before irradiation. The two pinning effects seem to be additive in that irradiation increases the hysteresis at all fields and the fishtail hump persists in the irradiated samples with roughly the same magnitude as before the damage channels are produced. For irradiated samples, there are two regions where pinning rises with increasing field, one near zero field due to a matching effect of the defect density with the vortex lattice spacing and a second at the same field as the original fishtail. Both effects appear in the same sample in different magnetic-field ranges. In order to assess the dependence of the fishtail on the defect size and concentration, Werner et al. [46] modified the defect structure by reactor neutron irradiation and additional annealing treatments. Their results emphasize the important role of normal conducting regions, which are created by clustering of defects, typically of oxygen vacancies. Non-Ohmic resistive state in $120Mev$ ^{16}O ion-irradiated $YBa_2Cu_3O_{7-\delta}$ has been studied by Iwase et al. [47]. They found a strong influence of the irradiation dose of fluence Φ on the power-like current-voltage characteristics $V \propto I^n$ with $n = f(T)\log(\Phi/\Phi_0)$. The effect of $2.5Mev$ electron irradiation on ceramic sintered $YBa_2Cu_3O_{7-\delta}$ was investigated by Gilchrist and Konczykowski [48]. They deduced a decrease of the characteristic magnetic field of Josephson junctions after irradiation and a very slight increase of intergrain critical current at very low doses. The authors noted that the accommodation of defects in the barrier region can lead to junction degradation and the loss of Josephson tunneling capability. More recently, He^+ irradiation effects on $YBa_2Cu_3O_{7-\delta}$ GBJJs modified by oxygen annealing have been studied by Navacerrada et al. [49, 50]. At the same time, Klaassen et al. [51] argue that natural linear defects in thin films form an analogous system to columnar tracks in irradiated samples. There are, however, three essential differences: (i) typical matching fields are at least one order of magnitude smaller, (ii) linear defects are smaller than columnar tracks, and (iii) the distribution of natural linear defects is nonrandom, whereas columnar tracks are randomly distributed.

3 Dislocation induced Josephson effect

To realize a scenario for the dislocation-induced atomic scale Josephson effect in HTS single crystals, let us consider the model of small Josephson contacts [52] with length $L < \lambda_J$ ($\lambda_J = \sqrt{\phi_0/\mu_0 l j_{c0}}$ is the Josephson penetration depth), in a strong enough magnetic field (which is applied normally to the contact area $l \times L$) such that $H > \phi_0/2\pi\lambda_J l$, where $l = \lambda_{L1} + \lambda_{L2} + t$ ($\lambda_{L1(2)}$ is the London penetration depth of the first (second) junction, and t is an insulator thickness). Assuming that twinning dislocations, lying along the z-axis (which

coincides with the direction of the applied magnetic field H) and distributed along the x-axis with dimensionless density $\rho(x)$, give rise to an (inhomogeneous) Josephson supercurrent density $j_c[\rho(x)]$, the critical current density through such an inhomogeneous single Josephson contact reads [53, 54]

$$j_s^J(\rho, H) = \frac{1}{L}\int_0^L dx j_c[\rho(x)]\sin(kx + c). \tag{1}$$

Here $k = 2\pi lH/\phi_0$, c is the zero-field phase difference between two superconductors forming a SIS-type Josephson contact, and we have assumed that the length of the contact L is the twin boundary (TB) length and the insulator thickness t corresponds to the TB thickness. Notice that the insulator thickness of the dislocation-induced Josephson junction, $t(x)$, is related to $\rho(x)$ as follows [54, 55, 56]

$$t(x) = \int_x^L dx'\rho(x') \tag{2}$$

Applicability of the dislocation description of a thin TB is known [13, 55] to be restricted by the condition $t \ll L$. As we shall see below, this condition is reasonably satisfied in dislocated HTS crystals. To proceed further, we postulate a δ-functional form of dislocation-induced critical current density assuming that $j_c[\rho(x)]$ is centered around an average (dimensionless) dislocation density ρ

$$j_c[\rho(x)] = j_{c0}e^{-t(x)/\xi_n}\delta[\rho(x) - \rho] \tag{3}$$

Here j_{c0} obeys the usual Ambegoakar-Baratoff expression for Josephson critical current [52], the exponential dependence accounts for the probability of Josephson tunneling on the local TB of thickness $t(x)$, and $\xi_n = \hbar v_F/\pi k_B T$ is the decay length of the contact. Taking into account the known property of the Dirac delta function $\delta[\rho(x) - \rho] = \delta[x - x_0(\rho)]/\mid \rho'(x) \mid_{x=x_0(\rho)}$ where $\rho'(x) \equiv d\rho/dx$, and $x_0(\rho)$ is the solution of the equation $\rho(x_0) = \rho$, Eqs.(1)-(3) give for the dislocation-induced single-junction critical current density

$$j_s^J(\rho, H) = j_s(\rho, 0)\sin\left(\frac{H}{H_\rho^J} + c\right), \tag{4}$$

where

$$j_s(\rho, 0) = j_{c0}\frac{\exp[-t(x_0)/\xi_n]}{L|\rho'(x_0)|}, \tag{5}$$

and

$$H_\rho^J = \left(\frac{L}{x_0}\right)H_0^J. \tag{6}$$

Here $x_0 = x_0(\rho)$ and $H_0^J = \phi_0/2\pi lL$ is a characteristic Josephson field.

To model a real situation of an inhomogeneous (due to the intragrain granularity) single crystal, let us consider a random network of dislocation-induced

Josephson junctions (JJ). Assuming, for simplicity, that JJ are randomly distributed according to the exponential law $P(l) = (1/l_0)\exp(-l/l_0)$ with l_0 being an average "sandwich" thickness, Eq.(4) results in the maximum (with $c = \pi/2$) critical current density for a granular superconductor [57]:

$$j_s(\rho, H) = \int_0^\infty dl P(l) j_s^J(\rho, H) = \frac{j_s(\rho, 0)}{1 + H^2/H_\rho^2}, \tag{7}$$

where $H_\rho = \phi_0/2\pi l_0 x_0(\rho)$. As is seen, Eq.(7), at least formally, describes the ordinary decrease of the critical current density with H. But actually this is not the case in view of the implicit dependence of a characteristic Josephson field H_ρ on the number of dislocations and on external sources (ω_0, see below) affecting the distribution of defects inside a crystal.

4 Screw dislocated thin films

4.1 Critical current density versus dislocation density

Supposing, for simplicity, the twinning boundaries (TB) as the only weak links sources, we are able to use for their treatment the dislocation model of elastic twinning [55] (see also the comprehensive review [13] and references therein). According to this model, the distribution of dislocations with density $\rho(x)$ along the elastic thin twin boundary is defined by the equilibrium condition under the influence of the external forces $\omega(x)$

$$\int_0^L \frac{dx'}{x' - x}\rho(x') = \omega(x), \tag{8}$$

where

$$\omega(x) = \frac{2\pi f(x)}{\mu b}. \tag{9}$$

Here, L is the twinning length, μ is the shear modulus of a dislocation, b is the magnitude of the Burgers vector, and $f(x)$ is a force affecting the distribution of dislocations within the TB. To make our consideration more definitive, let us discuss a concrete profile of the TB, i.e. solve the integral equation (8). If the dislocations are constrained only by external forces (the so-called freely growing TB), then the dislocation density distribution of such a growing TB is governed by the law [58]

$$\rho(x) = -\frac{1}{\pi^2}\sqrt{x(L-x)}\int_0^L \frac{dx'}{x' - x}\frac{\omega(x')}{\sqrt{x'(L-x')}} \tag{10}$$

In particular, for the case of the homogeneous external forces (with $\omega(x) \equiv \omega_0$), the above distribution near the TB tip reads (an example of inhomogeneous external forces, resulting in a self-tuned Josephson effect, is considered in [54])

$$\rho(x) = \rho_0\sqrt{1 - \frac{x}{L}}, \qquad \rho_0 \equiv \frac{\omega_0}{\pi} \tag{11}$$

The above expression is valid for $a_0 \leq x \leq L$, where a_0 is of the order of interatomic spacing. To describe correctly the vicinity of the TB origin ($x < a_0$), a more accurate treatment of Eq.(8) is needed. In view of Eqs.(5) and (6), distribution (11) results in the following explicit ρ dependencies of the zero-field critical current density

$$j_s(\rho, 0) = 2j_{c0}\left(\frac{\rho}{\rho_0^2}\right)\exp\left[-\left(\frac{b}{\xi_n}\right)\left(\frac{\rho}{\rho_0}\right)^3\right], \tag{12}$$

and characteristic Josephson field

$$H_\rho = H_0\frac{\rho_0}{1-(\rho/\rho_0)^2}, \tag{13}$$

respectively, where $H_0 = \phi_0/3\pi bl_0$. So, in view of Eq.(12), $j_s(\rho, 0)$ increases with ρ for $\rho < \rho_m$, has a maximum at $\rho = \rho_m \equiv \rho_0\sqrt[3]{\xi_n/3b}$, and then exponentially decreases for $\rho > \rho_m$. Using HTS parameters, $v_F \simeq 2 \times 10^5 m/s$, $T_c \simeq 90K$, and $b \simeq 1nm$, we get $\rho_m \simeq 1.2\rho_0$. On the other hand, according to the validity of distribution (11) and taking into account that usually $a_0/L < 10^{-2}$, we find that Eqs.(12) and (13) are valid for $0 \leq \rho/\rho_0 < 1$ only. It means that up to the highest admissible dislocation density (i.e., up to $\rho \simeq \rho_0$) we are always in the linear region (with $\rho < \rho_m$). Hence, in what follows the insignificant (in this region) exponential dependence of $j_s(\rho, 0)$ will be neglected.

Fig.1 shows the behavior of the dislocation-induced critical current density $j_s(\rho, H)/j_s(\rho, 0)$, calculated according to Eqs.(7), (12), and (13), versus applied magnetic field H/H_0 for various number of dislocations $n \equiv \rho/\rho_0$. Notice that at least in a qualitative agreement with the experimental observations in screw dislocated single crystals [23], Eqs.(7) and (13) suggest a linear (for small ρ) increase of the critical current density as well as a rather strong weakening of its field dependence (via the increase of the characteristic Josephson field, H_ρ) with the number of defects. It is worthwhile to mention that in view of the normalization condition $\int_0^L dx\rho(x) = b$ and Eq.(11), the length of the JJ contact L will be altered by external forces ρ_0, namely $L = 3b/2\rho_0$. In turn, due to the equilibrium equation (8), it means that within our scenario the number of dislocations ρ does not depend on external forces and is considered as a constant parameter. To estimate ρ_0, let us consider the pinning mechanism due to the screw dislocations. According to McElfresh et al. [59] (who treated the correlation of surface topography and flux pinning in YBCO thin films), the strain field of a dislocation can provide a mechanism by which the superconducting order parameter can be reduced, making it a possible site for core pinning. The elastic pinning mechanism could also be responsible for the large pinning forces associated with dislocation defects. There are two types of elastic pinning mechanisms possible, a first-order (parelastic) interaction and a second-order (dielastic) interaction. In the case of a screw plane defect, the parelastic pinning can be shown to be negligible [59]. However, the dielastic interaction comes about because the self-energy of a defect depends on the elastic constants of the material in which it forms. Since the crystalline material in a vortex core

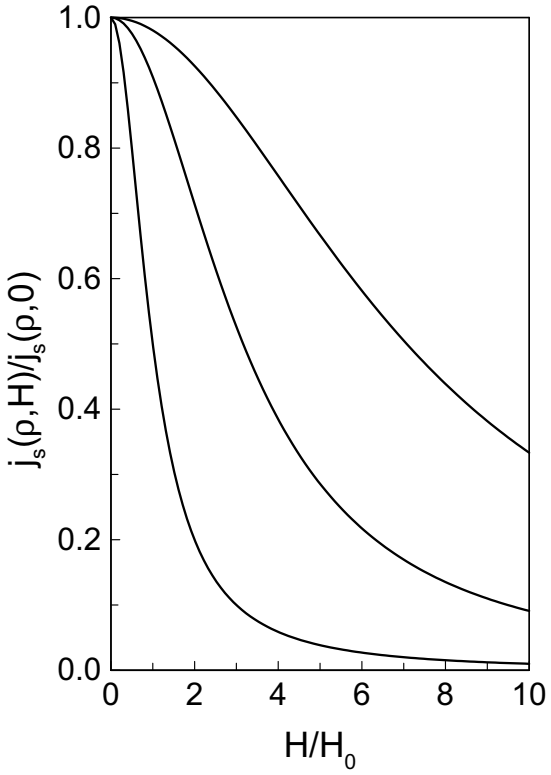

Figure 1: *Magnetic field dependence of the dislocation-induced critical current density for various values of the number of screw dislocations (increasing from bottom to top):* $n \equiv \rho/\rho_0 = 0.1; 0.5; 0.9$.

is stiffer, there is a higher energy bound up in the defect. For a tetragonal system with a screw dislocation, the energy density due to the defect strain is $(1/2)\mu\epsilon_{44}^2$, where μ is the shear modulus and ϵ_{44} is the shear strain. For a screw plane, $\epsilon_{44} \cong b/r$, where r is the distance from the center of the defect and b is the Burgers vector of the defect. The interaction energy density between the vortex and the screw plane is just $(1/2)\Delta\mu\epsilon_{44}^2$, where $\Delta\mu$ is the difference in shear modulus between superconducting and normal regions. For a vortex a distance r away from the defect, the interaction energy (per unit length of dislocation) reads

$$\mathcal{E}_d(r) = \frac{1}{2}\Delta\mu\epsilon_{44}^2(\pi\xi_0^2) \tag{14}$$

Setting $r \simeq \xi_0$, we get finally for the elastic force affecting the distribution of dislocations inside a crystal

$$f_{el} = \Delta\mu\left(\frac{b^2}{2\xi_0}\right), \tag{15}$$

which in view of Eqs.(10)-(12) results in $\rho_0 = 2f_{el}/\mu b = (b/\xi_0)(\Delta\mu/\mu)$. Taking the reported [59] for YBCO values of $\mu \simeq 10^{10} N/m^2$, $\Delta\mu = 10^{-5}\mu$, and $b \simeq \xi_0 \simeq 1\ nm$, we find that $f_{el} \simeq 5 \times 10^{-5} N/m$ and $\rho_0 \simeq 10^{-5}$. In turn, using $n_d \simeq 10^{13} m^{-2}$ for the maximum number of dislocations observed in screw dislocated thin films [21, 23, 60], which corresponds to our dimensionless quantity $\rho_{\rm exp} \simeq \pi b^2 n_d/4 \simeq 8 \times 10^{-6}$, we get $\rho_{\rm exp}/\rho_0 \simeq 0.8$. On the other hand, as it follows from Fig.1, for $H/H_0 = 5$ our model predicts $j_s(\rho, H)/j_s(\rho, 0) = 0.8$, which according to Eqs. (7) and (13) results in $\rho/\rho_0 \simeq 0.9$, in a good agreement with the observations. Furthermore, using the fact that in the above-mentioned experiments [23] substantial pinning enhancement due to screw dislocations has been observed for applied fields up to $H = 0.05$ T, we get $H_0 \simeq 0.01$ T for an estimate of the characteristic intrinsic Josephson field. Using [59] $\lambda_L \simeq 150$ nm for the zero-temperature London penetration depth in YBCO crystals, the above value of H_0 brings about the estimate of the length of the dislocation-induced intrinsic JJ contact $L \simeq 100nm$, that is $t \ll L < \lambda_J$ (where $t \simeq \xi_0$ is the TB insulator thickness and the Josephson penetration depth $\lambda_J \simeq 1\mu m$ for the intragrain critical current density $j_{c0} \simeq 10^{10} A/m^2$) in a satisfactory agreement with the applicability conditions for both the thin TB model [13] and the model of small Josephson junctions [52]. Moreover, since the vortex lattice parameter at $B = 0.05T$ is $a = \sqrt{\phi_0/B} \simeq 100nm$, a dislocation-induced Josephson contact (of length $L \simeq 100nm$) will indeed provide the optimum pinning center for applied fields up to $B = 0.05T$ [23]. It is worthwhile to mention that a pinning force per unit length $f_p = 10^{-4} N/m$ (which is of the same order of magnitude as the above-considered elastic force f_{el} acting upon dislocations), calculated in the single vortex limit, $f_p = j_{c0}\phi_0$, corresponds to a critical current density of $j_{c0} = 5 \times 10^{10} A/m^2$, in reasonable agreement with the j_{c0} found in dislocated YBCO thin films [23, 59].

4.2 Electric field effects

Let us consider now within our scenario a rather interesting phenomena observed in screw dislocated HTS thin films in the applied electric field [25, 61]. Since in ionic crystals dislocations can accumulate (or trap, due to the electric field around their cores) electrical charge along their length, application of an external electric field can sweep up these additional carriers, refreshing the dislocation cores, that is releasing the dislocation from a cloud of point charges (which, in field-free configuration, screen an electric field of the dislocation line for electrical neutrality). As is well-known [62, 63, 64] the charges on dislocations play a rather important role in charge transfer in ionic crystals. If a dislocation is oriented so that it has an excess of ions of one sign along its core, or if some ions of predominantly one sign are added to or removed from the end of half-plane, the dislocation will be charged. In thermal equilibrium it would be surrounded by a cloud of point defects of the opposite sign to maintain electrical neutrality. A screw dislocation can transport charge normal to the Burgers vector if it can carry vacancies with it. As Eshelby [64] pointed out, a dislocation resembles a surface in that it also can act as a source or sink of vacancies. Utilizing the

ionic (perovskite-like) nature of the HTS crystals [65], we propose a possible mechanism of the critical current enhancement in screw dislocated YBCO thin films [25] based on the electric-field induced converse piezoeffect due to the high polarizability of the defected medium in these materials. Piezoelectric effect, that is a transverse polarization induced by dislocation motion in ionic crystals, is certainly cannot be responsible for large field-induced effects in YBCO thin films because of too low rate of dislocation motion at the temperatures used in these experiments (another possibility to observe the direct piezoeffect in dislocated crystals is to apply an external stress field [62]). On the contrary, the converse piezoeffect, i.e., a change of dislocation-induced strain field in applied electric field can produce a rather considerable change of the critical current density in screw dislocated HTS thin films. Indeed, in applied electric field $\vec{E}$ the dislocation will be influenced by the external force $f_e(E) = b\sigma_e(E)$, where $\sigma_e(E) = \mu\epsilon_{44}(E)$ and the change of the dislocation-induced shear strain field in the applied electric field is defined as follows

$$\epsilon_{44}(E) = \epsilon_0\epsilon_r dE\cos\theta \tag{16}$$

Here d is the absolute value of the converse piezoeffect coefficient, θ stands for the angle between the screw dislocation line and the direction of an applied electric field, ϵ_r is the static permittivity which accounts for the long-range polarization of dislocated crystal (see below), and $\epsilon_0 = 8.85 \times 10^{-12} F/m$. According to Whitworth [62], the converse piezoeffect coefficient d in ionic dislocated crystals can be presented in the form

$$\frac{1}{d} = \frac{q\rho}{b} \tag{17}$$

Here ρ is the (dimensionless) dislocation density, and $q = e^*/w$ is the effective electron charge per unit length of dislocation w (in fact, w coincides with the thickness of the YBCO films [25]). Finally, due to Eq.(12) with $\rho_0(E) = (1 + 2f_e(E)/\mu b)$ and $f_e(E)$ given by Eqs.(16) and (17), electric-field induced change of the critical current density reads

$$j_s(\rho, \vec{E}) = 2j_c\frac{\rho}{\rho_0^2(\vec{E})} = j_s(\rho, 0)\left(1 + \frac{\mid \vec{E} \mid}{E_0(\rho)}\cos\theta\right)^{-2}, \tag{18}$$

where

$$j_s(\rho, 0) = 2j_c\frac{\rho}{\rho_0^2(0)}, \qquad E_0(\rho) = \frac{q\rho}{\epsilon_0\epsilon_r b}. \tag{19}$$

Here, $\rho_0(0) \equiv \rho_0(E = 0) = \Delta\mu/\mu$.

To attribute the above-mentioned mechanism to the field-induced changes of the critical current densities in dislocated YBCO thin films, we propose the following scenario [66]. Depending on the gate polarity, a strong applied electric field will result either in trapping the additional point charges by dislocation cores (when $\cos\theta = +1$) reducing the pinning force density, or in sweeping these point charges (surrounding the dislocation line to neutralize the net charge) up of the dislocation core (for the opposite polarity when $\cos\theta = -1$), thus increasing the core vortex pinning by fresh dislocation line. Using the fact that the

thickness w of YBCO thin films in the experiments carried out by Mannhart et al. [25] was $\simeq 70\dot{A}$, for the linear charge per length of dislocation we get the value $q = e^*/w = 2 \times 10^{-11} C/m$, that is $qb \simeq 0.1e^*$. To get an estimate of the threshold field $E_0(\rho)$, let us discuss the relationship between the above-introduced static permittivity of the dislocated crystal ϵ_r and the more recognized dielectric constant which in YBCO crystals is found [65] to be $\epsilon_{YBCO} \simeq 25$. Let S_{YBCO} be the crystal area, N_d the number of dislocations, and S_d the area occupied by a single dislocation line ($S_d \simeq \pi b^2$ where b is the magnitude of the Burgers vector). Then, approximately, $\epsilon_r/\epsilon_{YBCO} \simeq S_d N_d/S_{YBCO}$, or $\epsilon_r \simeq 4\rho\epsilon_{YBCO}$, where $\rho \simeq \pi b^2 N_d/4S_{YBCO}$ is the (dimensionless) dislocation density. Finally, using the maximum value of the dislocation density $n \simeq 4\rho/\pi b^2 \simeq 10^9 cm^{-2}$ observed in screw dislocated YBCO thin films [21, 23, 60], for an estimate of the threshold field $E_0(\rho)$ Eq.(19) predicts the value of $5 \times 10^5 V/cm$ which corresponds to the gate voltage $V_G = 25V$ and reasonably agrees with the typical values of the breakdown voltages used in the above-mentioned experiments. For self-consistency of the above-proposed scenario, it is important to mention that the induced (by applied electric field) polarization force f_e is compatible to the elementary pinning force f_p, introduced in the previous Section. Indeed, using the above-discussed parameters, we get from Eqs.(16)-(19) that for gate voltage $V_G = 25V$ and $\cos\theta = 1$, $f_e = enV_G/4 \simeq 10^{-5} N/m$. Let us briefly consider the influence of the applied magnetic field on the electric-field mediated converse piezoeffect. In view of Eqs.(13) and (16), external electric field will result in the following change of the characteristic field

$$\frac{H_\rho(\vec{E})}{H_\rho(0)} \simeq 1 - \left(\frac{\Delta H_\rho(0)}{H_0}\right)\left(\frac{\mid \vec{E} \mid}{E_0(\rho)}\right)\cos\theta, \tag{20}$$

where

$$\Delta H_\rho(0) \equiv H_\rho(0) - H_0, \tag{21}$$

and the characteristic fields $H_\rho(0)$ and H_0 are defined by Eqs.(13) and (8), respectively. As it follows from Eqs.(7), and (18)-(21), depending on the gate polarity the magnetic field dependence of the critical current density in dislocated crystals will be changed in a different way, in agreement with observations [25]. It is also worthwhile to mention that since recently a special attention has been given to the so-called electric field effects (FEs) in JJs and granular superconductors [67, 68, 69, 70, 71, 72]. The unusually strong FEs observed in bulk HTS ceramics [67] (including a substantial enhancement of the critical current, reaching $\Delta I_c(E)/I_c(0) = 100\%$ for $E = 10^7 V/m$) have been attributed to a crucial modification of the original weak-links structure under the influence of very strong electric fields. This hypothesis has been corroborated by further investigations, both experimental (through observation of the correlation between the critical current behavior and type of weak links [68]) and theoretical (by studying the FEs in SNS-type structures [69] and d-wave granular superconductors [70]). Among other interesting field induced effects, one can mention the FE-based Josephson transistor [71], Josephson analog of the *magnetoelectric effect* [72] (electric field generation of Josephson magnetic moment in zero

magnetic field), and recently predicted [73] giant enhancement of *nonlinear* (i.e. ∇T - dependent) thermal conductivity κ, reaching $\Delta\kappa(T,E)/\kappa(T,0) = 500\%$ for relatively low (in comparison with the fields needed to observe a critical current enhancement [67, 68]) applied electric fields E matching an intrinsic thermoelectric field $E_T = S_0|\nabla T|$, where S_0 is the Seebeck coefficient.

5 Fishtail anomaly (Peak effect)

5.1 Stoichiometric melt-textured crystals

Let us apply our scenario to discuss a possible origin of the so-called fishtail anomaly of the critical current density vs. applied magnetic field in stoichiometric melt-textured crystals possessing a large number of dislocations [34, 35]. As is well-known [13, 55], any external force leading to the redistribution of dislocations in the crystal, change the volume content of the martensite (superconducting) phase in HTS sample. Under an influence of external magnetic field, for instance, the dislocation will be affected by additional stress fields, σ_m, due to the differences between the magnetic susceptibilities of two phases. When one of these phases falls into the superconducting state, its magnetic properties will change drastically in the external magnetic field. If B_n and B_s are the magnetic inductions of the defect (normal) and superconducting regions, respectively, then such a dislocation will be influenced, in nonzero magnetic field, by a force (Cf. the electric-field induced force f_e from previous Section):

$$f_m = b\sigma_m = \frac{b}{2}\Delta BH. \tag{22}$$

Here $\Delta B = B_n - B_s$,$B_n = \mu_0 H$, $B_s = \mu_0 H + 4\pi M(H)$, and $\mu_0 = 4\pi\times 10^{-7} N/A^2$. To choose an appropriate form of the vortex lattice magnetization $M(H)$ sensitive to the magnetic anomalies at the region of $B \simeq 1T$, we note that according to our scenario, the strained regions near dislocation cores result in a lower $H^*_{c2}(T)$ as compared to the YBCO matrix $H_{c2}(T)$. Indeed, the order parameter Δ_{TB} near the TB is supposed to be reduced as compared to its bulk value Δ_0 as follows, $\Delta_{TB} = \Delta_0(b/\xi_n)$, where ξ_n is the decay length of the TB-induced Josephson contact. In turn, this leads to a similar depression of the superconducting coherence length $\xi_{TB} = \xi_0(\xi_n/b)$ and the upper critical field, $H^*_{c2}(T) \propto \phi_0/\xi^2_{TB} = H_{c2}(T)(b/\xi_n)^2$, where $H_{c2}(T) = H_{c2}(0)(1-T^2/T_c^2)$, $H_{c2}(0) \propto \phi_0/\xi_0^2$, and $\xi_0 = \hbar v_F/\pi\Delta_0$. Since for YBCO crystals, $\xi_0 \simeq 1nm$, $\mu_0 H_{c2}(0) \simeq 140T$, and $T_c \simeq 90K$, we get $H^*_{c2}(T) \simeq 2T$ for $T = 70K$. Thus, with a good accuracy we can use a high-field limit for vortex lattice magnetization (valid for $H \leq H^*_{c2}$), $4\pi M(H) = -\mu_0(H^*_{c2} - H)/2\kappa^{*2}$ where $\kappa^* = \kappa_0(b/\xi_n)^2$ is the Ginzburg-Landau parameter near the TB (recall that for YBCO $\kappa_0 \simeq 90$). According to Eqs.(7) and (13), dislocation-induced critical current density $j_s(\rho, H)$, driven by the magnetic-type external force (22), will exhibit a maximum at some field $H^*(\rho)$ which is defined as the solution of the balance equation $\rho_0(H^*) = \rho$, where $\rho_0(H) = 2f_m(H)/\mu b = \mu_0 H(H^*_{c2} - H)/2\mu\kappa^{*2}$. In view of the above-given ex-

plicit form of $\rho_0(H)$, the balance equation produces the following (dislocation-dependent) threshold field

$$H^*(\rho) = H^*_{c2}\left[1 - \sqrt{1 - \left(\frac{H_d}{H^*_{c2}}\right)^2}\right] \tag{23}$$

where $H_d = \sqrt{8\mu\rho\kappa^{*2}/\mu_0}$.

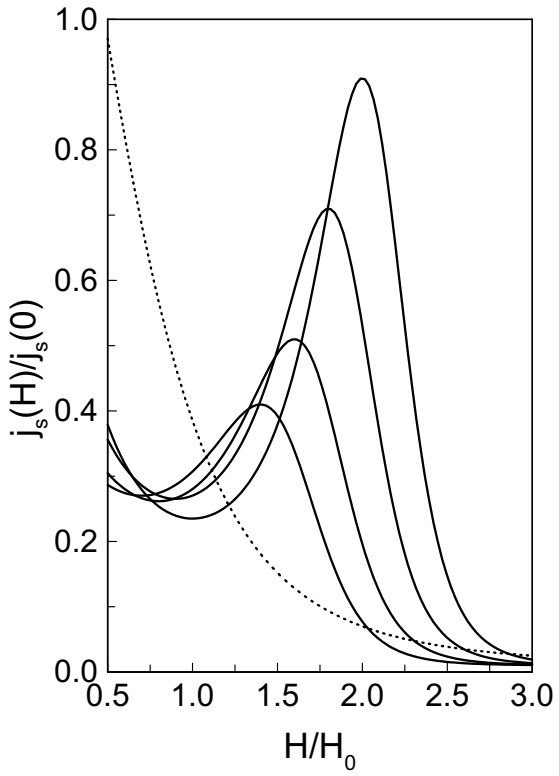

Figure 2: *The behavior of the normalized critical current density $j_s(H)/j_s(0)$ of melt-textured sample versus reduced magnetic field H/H_0 (peak effect) for various values of the number of dislocations (increasing from bottom to top): $n \equiv \rho/\rho_0 = 0.2; 0.5; 0.7; 0.9$. The dotted line corresponds to defect-free sample ($\rho = 0$).*

The existence of distinct magnetic properties along both sides of the twinning boundary leads, in nonzero magnetic field, to the growing of this twin through the crystal. This process can be stopped by the friction of dislocation via the crystalline lattice or by generation of an excess nonequilibrium concentration of (oxygen) vacancies (see the next Section). When the applied magnetic field reaches the threshold field $H^*(\rho)$, the moving dislocation is blocked, thus leading

to the adjustment of the defect structure to the penetrating vortex lines and, as a result, to the enhancement of the pinning forces and the recovery of the critical current density. When magnetic field overcomes this barrier, the pinning becomes less effective, and a rather smooth fall-off of the critical current is restored. Figure 2 depicts the predicted behavior of the normalized critical current density, $j_s(H)/j_s(0)$, of melt-textured sample versus reduced magnetic field H/H_0, calculated according to Eqs.(7), (12) and (13), for various values of the number of dislocations. Using $B^* = \mu_0 H^* \simeq 1T$ for the typical field region where anomalous fishtail behavior of critical currents has been observed [34, 35], we can estimate a number of dislocations n_{MT} needed to produce a peak-effect in stoichiometric melt-textured samples. Namely, taking $b \simeq 1nm$, $\mu \simeq 10^{10} N/m^2$, $\mu_0 H^*_{c2}(0) \simeq 5T$, and $\kappa^* \simeq 4$, we get $\mu_0 H_d \simeq 1T$ and $n_{MT} \simeq 4\rho/\pi b^2 \simeq 2 \times 10^8 cm^{-2}$ which is about 50% of the maximum number of dislocations found in the melt-textured materials [34, 35]. Finally, using the above parameters, we can estimate the magnitude of the magnetic force, f_m. The result for $B \simeq 1T$ is $f_m \simeq 2 \times 10^{-5} N/m$ which is quite comparable with the elementary pinning force density f_p, elastic force f_{el}, and electric field polarization force f_e.

5.2 Deoxygenated single crystals

To apply the above-considered scenario for the description of the anomalous magnetic behavior observed in the oxygen-deficient single crystals, we should take into account existence of a rather important force of inelastic origin (so-called osmotic force f_0) which, together with the above-mentioned magnetic force, f_m, will define the ultimate defect structure of these crystals. The origin of this force in deoxygenated crystals is due to an excess nonequilibrium concentration of oxygen vacancies c_v (with $c_v \neq 1$). Unlike the ordinary oxygen diffusion $D = D_0 e^{-U_d/k_B T}$ in $YBa_2Cu_3O_{7-\delta}$ which is extremely slow even near T_c (due to a rather high value of the activation energy U_d in these materials, typically $U_d \simeq 1eV$), the osmotic (pumping) mechanism [74] can substantially facilitate oxygen transport in underdoped crystals (with oxygen-induced dislocations). This mechanism relates a local value of the chemical potential (chemical pressure) $\mu(\mathbf{x}) = \mu(0) + \nabla\mu \cdot \mathbf{x}$ with a local concentration of point defects as follows $c(\mathbf{x}) = e^{-\mu(\mathbf{x})/k_B T}$. Indeed, when in such a crystal there exists a nonequilibrium concentration of vacancies, dislocation is moved for atomic distance b by adding excess vacancies to the extraplane edge and as a result the force f_o produces the work bf_o. The produced work is simply equal to the chemical potential of added vacancies, so that $bf_o = \mu_v/b$. What is important, this mechanism allows us to explicitly incorporate the oxygen deficiency parameter δ into our model by relating it to the excess oxygen concentration of vacancies $c_v \equiv c(0)$ as follows $\delta = 1 - c_v$ (in most interesting cases $\delta \ll 1$). As a result, the chemical potential of the single vacancy reads $\mu_v \equiv \mu(0) = -k_B T \log(1-\delta)$, leading to the following explicit form of the osmotic force [75, 76, 77]

$$f_0 = -\frac{k_B T}{b^2} \log(1-\delta) \simeq \frac{k_B T}{b^2} \delta. \tag{24}$$

Remarkably, the same osmotic mechanism was used by Gurevich and Pashitskii [78] to discuss the modification of oxygen vacancies concentration in the presence of the TB strain field. Let us consider influence of two competitive forces, f_m and f_0, on the magnetic field critical current behavior. In accordance with Eqs.(9), (12), and (22), the external force dependent part of the dislocation density, ρ_0, reads

$$\rho_0(\delta, H) = \rho_0(\delta, 0)\left[1 + \frac{H(H^*_{c2} - H)}{H^2_\delta}\right], \tag{25}$$

where

$$\rho_0(\delta, 0) \equiv \frac{2k_BT}{b^3\mu}\delta, \qquad H_\delta \equiv \sqrt{\frac{4k_BT\kappa^{*2}\delta}{b^3\mu_0}}. \tag{26}$$

Thus, the non-zero oxygen deficiency (which is responsible for the sample non-stoichiometry) results in an intrinsic characteristic field, H_δ, which reflects a subtle balance between extended (dislocations) and point (oxygen vacancies) defects in a given sample. In view of Eqs.(7) and (13), the above $\rho_0(\delta, H)$ brings about the following explicit dependence of the dislocation-induced critical current density

$$j_s(H) = 2j_{c0}(\delta)\frac{\rho}{\rho^2_0(\delta, H)}\left[1 + \left(\frac{H}{H_0}\right)^2\left(1 - \left(\frac{\rho}{\rho_0(\delta, H)}\right)^2\right)^2\right]^{-1} \tag{27}$$

Here we have taken into account that according to the observations [31] $j_{c0}(\delta) \simeq j_{c0}(0)(1 - \delta)$. Fig.3 illustrates the evolution of $j_s(H)/j_s(0)$ versus applied magnetic field H/H_0 with increasing the oxygen deficiency δ (for $\rho = \rho_0(\delta, 0)$). As is seen, below some threshold concentration of oxygen defects, δ_c, critical current density exhibits a peak-like behavior. The peak is shifted to lower fields with increasing the oxygen deficiency and disappears at $\delta = \delta_c$, in agreement with the observations. Due to Eqs.(25)-(27), $j_s(H)$ passes through the maximum above some threshold field, $H^*(\delta, T)$, which is defined via the balance equation $\rho_0(\delta, H^*) = \rho$. Taking into account the explicit form of $\rho_0(\delta, H)$ (see Eqs.(25)), the threshold field reads

$$H^*(\delta, T) = H^*_{c2}\left[1 - \sqrt{1 - \left(\frac{H_d}{H^*_{c2}}\right)^2\left(1 - \frac{\delta}{\delta_c}\right)}\right], \tag{28}$$

or alternatively

$$H^*(\delta, T) = H^*_{c2}\left[1 - \sqrt{1 - \left(\frac{H_d}{H^*_{c2}}\right)^2\left(1 - \frac{T}{T_0}\right)}\right], \tag{29}$$

where

$$\delta_c \equiv \frac{\mu b^3\rho}{2k_BT}, \qquad T_0 \equiv \frac{\mu b^3\rho}{2k_B\delta}. \tag{30}$$

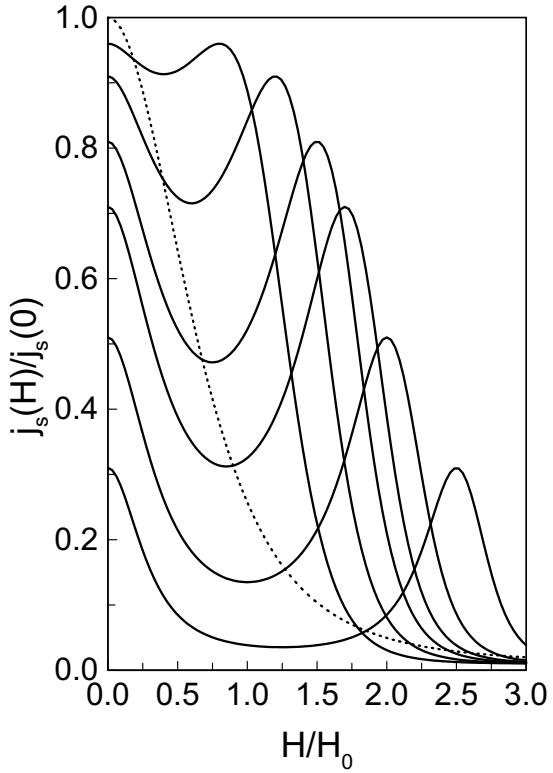

Figure 3: *The behavior of the normalized critical current density $j_s(H)/j_s(0)$ versus reduced magnetic field H/H_0 for various values of the oxygen deficiency parameter (increasing from top to bottom): $\delta = 0.01; 0.05; 0.07; 0.1; 0.15; 0.2$. The dotted line corresponds to stoichiometric sample ($\delta = 0$).*

Thus, in addition to the strong δ-dependence, Eq.(28) predicts decrease of the peak-effect threshold field, $H^*(\delta, T)$, with increasing the temperature as well, also in agreement with the observations [27, 28, 29, 30, 31]. Taking $b \simeq 1nm$, $\delta_c = 0.23$, $\mu_0 H_d \simeq 1T$, and $\mu_0 H^*_{c2}(T = 70K) \simeq 2T$, for $\delta = 0.05$ and $T = 70K$ we obtain the estimate of the threshold field $B^* = \mu_0 H^* \simeq 1T$, which is very close to the fields where the anomalous phenomena in $YBa_2Cu_3O_{7-\delta}$ single crystals have been observed [28]. According to Eq.(24), the above estimates predict $f_o \simeq 5 \times 10^{-5} N/m$ for the osmotic force magnitude. At the same time, using the experimentally found [30] critical value of oxygen deficiency $\delta_c = 0.23$, Eq.(30) suggests an estimate of the number of dislocations, n_{DO}, needed to produce the above-discussed critical current enhancement (fishtail anomaly) in deoxygenated HTS single crystals. Namely, for $T = 70K$ and $\mu = 10^{10} N/m^2$, we get $n_{DO} \simeq 4\rho/\pi b^2 \approx 2 \times 10^6 cm^{-2}$. Notice that this is only 1% of the number of defects n_{MT} needed to produce the fishtail anomaly in well-oxygenated

melt-textured crystals (see the previous Section). It means, in fact, that in contrast to the melt-textured case, in oxygen-depleted single crystals dislocations play an auxiliary (as compared to the points defects, oxygen vacancies), yet important role, providing a background for oxygen defects redistribution inside a crystal and thus adjusting the pinning ability of the material. A rather strong correlation between dislocations and oxygen defects is seen also through ρ-dependence of the critical oxygen deficiency parameter δ_c (see Eq.(30)). The latter parameter has a simple physical meaning. Namely [30], for $\delta > \delta_c$ oxygen-rich superconducting grains are separated by oxygen-poor insulating boundaries so that there is no superconducting path through the sample. Notice also (by comparing the low field regions in Fig.3 for different δ) that at a given number of dislocations, increase of oxygen defects leads to a more flat behavior of the critical current at small fields indicating that point defects are the major pinning centers in this region [27]. In a similar way, T_0 plays a role of the phase-locking temperature above which the superconductivity between oxygen-rich grains is suppressed and the fishtail phenomenon disappears. For the above-mentioned parameters this characteristic temperature is estimated to be $T_0 \simeq 87K$. It is interesting also to mention the experiments on electromigration of oxygen in HTS single crystals conducted by Moeckly et al. [79]. They have observed that the superconducting properties of the disordered regions caused by electromigration are indicative of a filamentary superconductive system shunted by nonsuperconductive Ohmic parts. If we assume, after Moeckly et al. [79], that the so-called electron-wind contribution dominates the phenomenon, the electromigration force acting on the oxygen ions reads

$$f_{em} = \frac{2mv_F\sigma}{be} J_{em}. \tag{31}$$

Here J_{em} is the applied critical current density, v_F is the Fermi velocity, and σ is the oxygen ion scattering cross section. Taking into account the values of the parameters used in the above-mentioned experiments [79], namely $J_{em} = 5 \times 10^6 A/cm^2$, $v_F = 2 \times 10^7 cm/s$, and $\sigma \approx b^2 \approx 10^{-14} cm^2$, we get for an estimate of the electromigration force $f_{em} \simeq 10^{-4} N/m$. Remarkably, this force is of the same order of magnitude as the above-considered magnetic and osmotic forces. Besides, the described in this Section scenario has been used [80] to explain the observed [81] irreversibility line $T_c(H)$ crossover (between Almeida-Thouless and Gabay-Toulouse behavior) in deoxygenated HTS. And finally, a few novel interesting effects in intrinsically granular non-stoichiometric material have been recently predicted [82], including Josephson chemomagnetism (chemically induced magnetic moment in zero applied magnetic field) and its influence on a low-field magnetization (chemically induced paramagnetic Meissner effect), and magnetoconcentration effect (creation of extra oxygen vacancies in applied magnetic field) and its influence on a high-field magnetization (chemically induced analog of fishtail anomaly).

6 Irradiated single crystals

There are two possibilities to adapt our scenario for a qualitative description of the anomalous magnetic phenomena observed in irradiated HTS single crystals. We can either consider the well-aligned tracks of damaged material, produced by particle irradiation, as potential sources of intragrain weak links (provided that the track's diameter is of the order of the coherence length [77]) or, alternatively, exploit the well-known [83, 84] fact that irradiation produces a large density of extended defects (in particular, dislocations) in these materials. The experiments revealed that there is some threshold magnetic field, $H^*(\Phi)$, which is almost linearly increases with the fluence Φ and above which a substantial increase of the critical current density, $j_s(\Phi, H)$, has been observed [41, 42]. Besides, it was found that the magnitude of fluence, $\Phi^*(H)$, which optimizes $j_s(\Phi, H)$, increases almost linearly with the applied field. As it was observed [43], the strain and structural disorder of the amorphous region propagates into the crystal lattice in a direction normal to the ion track. It means that, for an isolated amorphous track, a radially symmetric displacement field $u(r) \simeq E_{eff}(R^2/r)$ (where R is the radius of the amorphous track, and for YBCO $E_{eff} \simeq 0.02$) occurs in the matrix around the ion track (Cf. the appearance of a displacement field around a screw dislocation). According to Weaver et al. [84], irradiation of fluence Φ induces the network of dislocations of density $n(\Phi) = n(0) + n_m(1 - \exp(-\alpha\Phi))$, where $n(0)$ is the dislocation density of a virgin (pre-irradiated) sample, n_m the maximum density after irradiation, and α is the so-called displacement cross section which is related to the number of displaced atoms per particle per unit length. Assuming that $\alpha\Phi \ll 1$ (which is usually the case for real experiments), in the dimensionless units the above equation reads $\rho(\Phi) \simeq \rho(0) + \alpha\Phi$, where $\rho(\Phi) \equiv n(\Phi)/n_m$ and $\rho(0) \equiv n(0)/n_m$. Let us consider the magnetic field behavior of the critical current density, $j_s(\Phi, H)$, upon irradiation. According to our scenario for weak-links-mediated critical current enhancement in defected samples, the irradiation-induced behavior of $j_s(\Phi, H)$ will show the same peculiarities we have discussed earlier considering the fishtail anomaly in melt-textured and deoxygenated crystals. Indeed, in view of the fluence dependence of the characteristic field H_ρ (through $\rho(\Phi)$, see Eq.(13)), it is easy to verify that $j_s(\Phi, H)$ will have a maximum at some threshold field, $H^*(\delta, \Phi)$, which is defined (by analogy with the threshold field for oxygen-deficient sample, Cf. Eq.(28)) as the solution of the balance equation $\rho_0(H^*, \delta) = \rho(\Phi)$. Taking into account the definitions of $\rho_0(\delta, H)$, given by Eqs.(25) and (26), and $\rho(\Phi)$, the above balance equation results in the following threshold field

$$H^*(\delta, \Phi) = H^*_{c2}\left[1 - \sqrt{1 - \left(\frac{H_d(\delta)}{H^*_{c2}}\right)^2 \left(1 + \frac{\Phi}{\Phi^*(\delta, 0)}\right)}\right], \qquad (32)$$

where

$$\Phi^*(\delta,0)=(\delta_c-\delta)\Phi_0^*, \qquad \Phi_0^*=\frac{2k_BT}{\alpha\mu b^3}. \tag{33}$$

Here $H_d(\delta)=H_d\sqrt{1-\delta/\delta_c}$ with δ_c and H_d still governed by Eqs.(28)-(30) but with $\rho\equiv\rho(0)$. Alternatively, we can introduce an optimum (maximum) value of the fluence, $\Phi^*(\delta,H)$, as the solution of the equation $\rho_0(H,\delta)=\rho(\Phi^*)$. The result is as follows

$$\Phi^*(\delta,H)=\Phi^*(\delta,0)\left[1+\frac{H(H_{c2}^*-H)}{H_d^2(\delta)}\right] \tag{34}$$

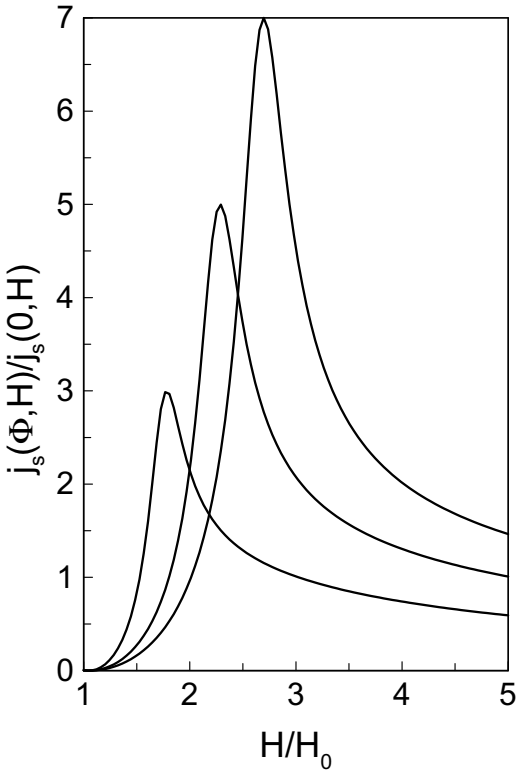

Figure 4: *The behavior of the normalized critical current density $j_s(\Phi,H)/j_s(0,H)$ versus reduced magnetic field H/H_0 for various values of the reduced irradiation fluence (increasing from bottom to top): $\Phi/\Phi_0=1;5;10$.*

Turning to the discussion of the above-obtained model predictions, we notice that they cover practically all the peculiarities observed in irradiated single crystals. Indeed, in view of Eqs.(7) and (13), the irradiation-induced critical

current density reads

$$j_s(\Phi,H)=2j_{c0}(\Phi)\frac{\rho(\Phi)}{\rho_0^2(\delta,H)}\left[1+\left(\frac{H}{H_0}\right)^2\left(1-\left(\frac{\rho(\Phi)}{\rho_0(\delta,H)}\right)^2\right)^2\right]^{-1} \qquad (35)$$

Here we have taken into account the possibility of deterioration of the pre-irradiated weak links (due to another defects) upon irradiation. Within the same accuracy ($\alpha\Phi \ll 1$), experiments [85] revealed that $j_{c0}(\Phi) \simeq j_{c0}(0)(1-\sqrt{\alpha\Phi})$. Let us consider first the case of nearly fully oxygenated pre-irradiated samples (with $\delta \simeq 0$). Fig.4 depicts the calculated dependence of the critical current density $j_s(\Phi,H)/j_s(0,H)$ upon applied magnetic field H/H_0 for various values of the irradiation fluence Φ/Φ_0 (with $\Phi_0=\rho(0)/\alpha$). As is seen, a pronounced peak appears which is shifted to higher magnetic fields with increasing the irradiation fluence. And this model prediction is also in agreement with the observations.

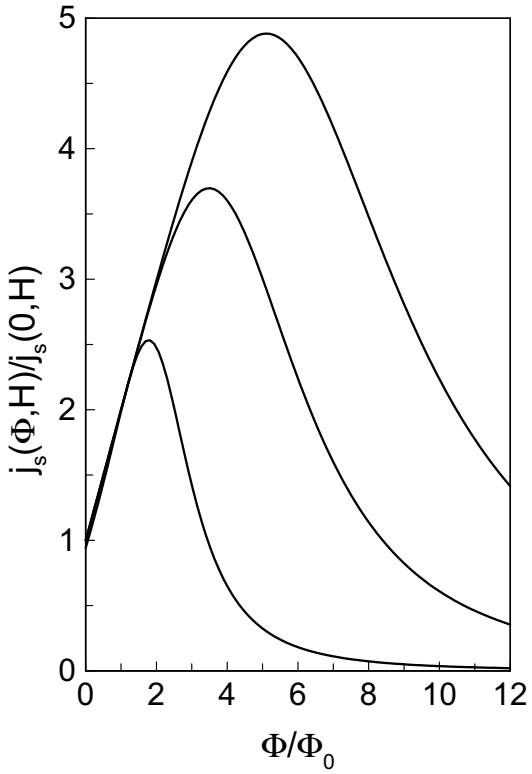

Figure 5: *The behavior of the normalized critical current density $j_s(\Phi,H)/j_s(0,H)$ versus reduced irradiation fluence Φ/Φ_0,calculated according to Eq.(35), for various values of the reduced magnetic field (increasing from bottom to top): $H/H_0=1;2;3$.*

In turn, Fig.5 shows the behavior of $j_s(\Phi, H)/j_s(0, H)$ versus irradiation fluence Φ/Φ_0 for different values of the applied magnetic field H/H_0, calculated according to Eqs.(35) and (25). Notice a tremendous increase of the critical current density with fluence (especially at high magnetic fields where the irradiation-induced defect structure is supposed to match optimally the vortex lattice structure). The magnitude of the peak, $\Phi^*(H)$, is seen to shift to higher fluences with increasing the field, in agreement with observations [41, 42]. Using the experimental data of Hardy et al. [41, 42] for the threshold fields at different fluences, namely $B^*(\Phi = 10^{11} cm^{-2}) = 1T$ and $B^*(\Phi = 3 \times 10^{11} cm^{-2}) = 2T$, we get from Eqs.(32) and (33) $\Phi_0 \simeq 5 \times 10^{10} cm^{-2}$. Furthermore, using a typical value of $\alpha \simeq 7 \times 10^{-17} cm^2$ [84], we can get an estimate of the defect number density in pre-irradiated sample. The result is as follows, $n(0) \simeq 4\rho(0)/\pi b^2 \simeq 2 \times 10^8 cm^{-2}$. Turning to the optimum value of the fluence, $\Phi^*(H)$, which has been measured during the same experiments [41, 42], we deduce the following estimates: $\Phi^*(B = 1T) = 5 \times 10^{10} cm^{-2}$ and $\Phi^*(B = 2T) = 3 \times 10^{11} cm^{-2}$. In view of Eq.(34), the above values predict a reasonable value for the intrinsic characteristic field $B^*(0, 0) \simeq 1T$. Let us briefly consider the case when pre-irradiated sample is in a highly oxygen-deficient state (with $\delta \simeq \delta_c$). Since $\Phi^*(\delta, 0) = (\delta_c - \delta)\Phi_0^*$, it means that a less value of the fluence is required to be applied to the deoxygenated sample to get the same (as for fully oxygenated sample) optimum properties of the critical current density in irradiated sample. This conclusion is in agreement with some recent experimental observations [43, 86, 87, 88, 89]. For example, Zhu et al. [43] have observed that the extent of radiation damage strongly depends on the stoichiometry of the sample. They found that an average diameter of the amorphous region for $YBa_2Cu_3O_{7-\delta}$ crystals was $2R \simeq 7.8$ nm, 5.3 nm, and 3.3 nm for $\delta \simeq 0.7$, 0.3, and 0.01, respectively. Moreover, in oxygenated samples the irradiation-induced damage was found [43] to be much less profound than that in oxygen-deficient samples.

It is worthwhile to mention that a somewhat similar concept of weak-links induced vortex pinning has been also considered by Lee et al. [90]. Using a Monte-Carlo technique within a 3-D model of Josephson junction arrays (JJAs), they found a substantial increase of critical current densities due to the flux pinning by columnar defects (for discussion of many other interesting effects in JJAs, see, e.g., a recent review [91]). Besides, the suggested in this Section scenario can also be responsible for the observed [48] fluence induced shift in the irreversibility line (via the Φ dependence of the threshold field $H^*(\Phi)$) [77] and allows to interpret the experimental data on Φ dependence of the power-like current-voltage characteristics and non-Ohmic resistive states in heavy-ion irradiated $YBa_2Cu_3O_{7-\delta}$ crystals [47, 77].

7 Conclusion

In summary, a unified approach for description of the critical current density improvement in dislocated, deoxygenated, and irradiated superconductors was proposed based on intrinsic Josephson effect which is supposed to be active in

HTS materials. The model is based on the existence of various competitive forces affecting a rather delicate balance between extended (dislocations) and point (oxygen vacancies) defects inside a crystal. The scenario incorporates the idea of a quite strong correlation between the intragrain weak links and vortex pinning, and implies that practically any treatment of the superconducting sample (such as sintering, melt-texturing, silver coating, thermal and mechanical treatment, oxygenation/deoxygenation process, particle irradiation, application of high magnetic and electric fields, etc) will inevitably result in the rearrangement of the pre-treated defect structure of the material to optimize its pinning ability as well as its vital critical parameters (such as critical temperature, critical fields, critical current density, magnetization, etc) [92]. Table I summarizes the external forces acting on dislocations (including the equivalent elementary pinning force f_p), considered in the present paper, as well as their estimates according to the corresponding parameters deduced from the literature. Notice that all of them are of the same order of magnitude supporting thus the idea of unification of different physical phenomena related to the critical current density improvement in high-temperature superconductors.

Table 1: *The external forces affecting the defect structure arrangement within a sample: equivalent elementary pinning force (f_p), elastic force (f_{el}), magnetic force (f_m), electric force (f_e), osmotic force (f_o), electromigration force (f_{em}), and analog of irradiation force (f_ϕ).*

Forces	**Parameters**
$f_p = j_c\phi_0 \simeq 2\times10^{-5}N/m$	$j_c = 10^{10}A/m^2$, $\phi_0 = 2\times10^{-15}Wb$
$f_{el} = \left(\frac{b}{2}\right)\Delta\mu \simeq 5\times10^{-5}N/m$	$\Delta\mu = 10^5N/m^2$, $b = 1nm$
$f_m = \left(\frac{b}{2}\right)\Delta BH \simeq 3\times10^{-5}N/m$	$\Delta B \simeq \mu_0 H \simeq 1T$, $b = 1nm$
$f_e = \left(\frac{1}{4}\right)enV_G \simeq 4\times10^{-5}N/m$	$V_G = 25V$, $n = 10^{13}m^{-2}$
$f_o = \left(\frac{k_BT}{b^2}\right)\delta \simeq 5\times10^{-5}N/m$	$\delta = 0.05$, $b = 1nm$, $T = 70K$
$f_{em} = \left(\frac{mv_Fb}{e}\right)J_{em} \simeq 10^{-4}N/m$	$J_{em} = 10^{10}A/m^2$, $v_F \simeq 10^5m/s$
$f_\phi \simeq \left(\frac{b\phi_0^2}{2\mu_0}\right)n_\Phi^2 \simeq 2\times10^{-5}N/m$	$n_\Phi \simeq 10^{14}m^{-2}$, $b = 1nm$

ACKNOWLEDGMENTS

Very useful discussions on the subject matter with Fernando Araujo-Moreira, Marcel Ausloos, John Clem, Guy Deutscher, Mauro Doria, Ted Geballe, Ken Gray, Vladimir Gridin, Alex Gurevich, Jorge José, David Larbalestier, Franc Nabarro, Anant Narlikar, Terry Orlando, Wilson Ortiz, Paulo Pureur, Jacob Schaf, Donglu Shi, James Thompson and Michael Tinkham are highly appreciated.

References

[1] Terry P. Orlando and Kevin A. Delin, *Foundations of Applied Superconductivity* (Addison-Wesley, 1991).

[2] G. Deutscher, IBM J. Res. Develop. **33**, 293 (1989).

[3] *Physics and Materials Science of Vortex States, Flux Pinning and Dynamics*, NATO Advanced Studies Institute Series, vol.**356E**, edited by. R. Kossowsky et al. (Kluwer Academic, Dordrecht, The Netherlands, 1999).

[4] Special issue on flux pinning in *Studies of High Temperature Superconductors*, vol.**32**, edited by A. Narlikar (Nova Science, New York, 2000).

[5] G. Deutscher and K.A. Müller, Phys. Rev. Lett. **59** (1987) 1745.

[6] W. Schnelle, E. Braun, H. Broicher, H. Weiss, H. Geus, S. Ruppel, M. Galffy, W. Braunisch, A. Waldorf, F. Seider, and D. Wohlleben, Physica C **161**, 123 (1989).

[7] M. Hervieu, C. Caegnaert, R. Retoux, and B. Raveau, Materials Sci. Engineering B **6**, 211 (1990).

[8] Y. Zhu, M. Suenaga, Y. Xu, R.L. Sabatini, and A.R. Moodenbaugh, Appl. Phys. Lett. **54**, 374 (1989).

[9] Y. Zhu, M. Suenaga, and Y. Xu, Phil. Mag. Lett. **60**, 51 (1989).

[10] S. Amelinckx, J. Less-Comm. Met. **150**, 71 (1989).

[11] G. van Tendeloo, D. Broddin, H.W. Zandbergen, and S. Amelinckx, Physica C **167**, 627 (1990).

[12] H.W. Zandbergen, J. Superconduct. **2**, 337 (1989).

[13] V.S. Boiko and A.M. Kosevich, Sov. J. Low. Temp. Phys. **17**, 3 (1991).

[14] J.G. Darab, R.E. MacCrone, and K. Rajan, Physica C **173**, 213 (1991).

[15] F.W. Gayle and D.L. Kaiser, J. Mater. Res. **6**, 908 (1991).

[16] S.E. Babcock and D.C. Larbalestier, J. Mater. Res. **5**, 919 (1990).

[17] X.Y. Cai, A. Gurevich, I.F. Tsu, D.L. Kaiser, S.E. Babcock, and D.C. Larbalestier, Phys. Rev. B **57**, 10951 (1998).

[18] I.F. Tsu, J.-L. Wang, D.L. Kaiser, and S.E. Babcock, Physica C **306**, 163 (1998).

[19] A. Diaz, L. Mechin, P. Berghuis, and J.E. Evetts, Phys. Rev. Lett. **80**, 3855 (1998).

[20] P. Shang, G. Yang, I.P. Jones, C.E. Gough, and J.S. Abell, Appl. Phys. Lett. **63**, 827 (1993).

[21] Ch. Gerber, D. Anselmetti, J.G. Bednorz, J. Mannhart, and D.G. Schlom, Nature (London) **360**, 279 (1991).

[22] C.H. Chen, J. Kwo, and M. Hong, Appl. Phys. Lett. **52**, 841 (1988).

[23] J. Mannhart, D. Ansehnetti, J.G. Bednorz, A. Catana, Ch. Gerber, K.A. Müller, and D.G. Schlom, Z. Phys. B **86**, 177 (1992).

[24] R. Hlubina, M. Grajcar, V. Bezak, P. Guba, and K. Karlovsky, Physica C **329**, 5 (2000).

[25] J. Mannhart, D.G. Schlom, J.G. Bednorz, and K.A. Müller, Phys. Rev. Lett. **67**, 2099 (1991).

[26] K.M. Lang, V. Madhavan, J.E. Hoffmann, E.W. Hudson, H. Eisaki, S. Uchida, and J.C. Davis, Nature (London) **415**, 412 (2002).

[27] G. Yang, P. Shang, S.D. Sutton, I.P. Jones, J.S. Abell, and C.E. Gough, Phys. Rev. B **48**, 4054 (1993).

[28] M. Daeumling, J.M. Seuntjens, and D.C. Larbalestier, Nature (London) **346**, 332 (1990).

[29] J.L. Vargas and D.C. Larbalestier, Appl. Phys. Lett. **60**, 1741 (1992).

[30] M. Osofsky, J.L. Cohn, E.F. Skelton, M.M. Miller, R.J. Soulen, Jr., S.A. Wolf, and T.A. Vanderah, Phys. Rev. B **45**, 4916 (1993).

[31] J.G. Ossandon, J.R. Thompson, D.K. Christen, B.C. Sales, H.R. Kerchner, J.O. Thomson, Y.R. Sun, K.W. Lay, and J.E. Tkaczyk, Phys. Rev. B **45**, 12534 (1992).

[32] L. Klein, E.R. Yacoby, Y. Yeshurun, A. Erb, G. Müller-Vogt, V. Breit, and H. Wuhl, Phys. Rev. B **49**, 4403 (1994).

[33] J.G. Ossandon, J.R. Thompson, D.K. Christen, B.C. Sales, Y. Sun, and K.W. Lay, Phys. Rev. B **46**, 3050 (1992).

[34] M. Ullrich, D. Müller, W. Mexner, M. Steins, K. Heinemann, and H.C. Freyhardt, Phys. Rev. B **48**, 7513 (1993).

[35] M. Ullrich, D. Müller, K. Heinemann, L. Niel, and H.C. Freyhardt, Appl. Phys. Lett. **63**, 406 (1993).

[36] F. Sandiumenge, N. Vilalta, J. Rabier, and X. Obradors, Phys. Rev. B **64**, 184515 (2001).

[37] M. Jirsa, L. Pust, D. Dlouhy, and M.R. Koblischka, Phys. Rev. B **55**, 3276 (1997).

[38] T. Banerjee, D. Kanjilal, and R. Pinto, Phys. Rev. B **65**, 174521 (2002).

[39] L. Civale, A.D. Marwick, M.W. McElfresh, T.K. Worthington, A.P. Malozemoff, F.H. Holtzberg, J.R. Thompson, and M.A. Kirk, Phys. Rev. Lett. **65**, 1164 (1990).

[40] L. Civale, M.W. McElfresh, A.D. Marwick, F.H. Holtzberg, C. Field, J.R. Thompson, and D.K. Christen, Phys. Rev. B **43**, 13732 (1991).

[41] V. Hardy, D. Groult, J. Provost, M. Hervieu, and B. Raveau, Physica C **178**, 255 (1991).

[42] V. Hardy, D. Groult, J. Provost, and B. Raveau, Physica C **190**, 289 (1992).

[43] Y. Zhu, Z.X. Cai, R.C. Budhani, M. Suenaga, and D.O. Welch, Phys. Rev. B **48**, 6436 (1993).

[44] M. Li, C.J. van der Beek, M. Konczykowski, H.W. Zandbergen, and P.H. Kes, Phys. Rev. B **66**, 14535 (2002).

[45] Ming Xu, J.E. Ostenson, D.K. Finnemore, M.J. Kramer, J.A. Fendrich, J.D. Hettinger, U. Welp, G.W. Crabtree, B. Dabrowski, and K. Zhang, Phys. Rev. B **53**, 5815 (1996).

[46] M. Werner, F.M. Sauerzopt, H.W. Weber, and A. Wisniewski, Phys. Rev. B **61**, 14795 (2000).

[47] A. Iwase, N. Masaki, T. Iwata, and T. Nishira, Physica C **174**, 321 (1991).

[48] J. Gilchrist and M. Konczykowski, Physica C **168**, 123 (1990).

[49] M.A. Navacerrada, M.L. Lucia, and F. Sanchez-Quesada, Phys. Rev. B **61**, 6422 (2000).

[50] M.A. Navacerrada, M.L. Lucia, and F. Sanchez-Quesada, Europhys. Lett. **54**, 387 (2001).

[51] F.C. Klaassen, G. Doornbos, J.M. Huijbregtse, R.C.F. van der Geest, B. Dam, and R. Griessen, Phys. Rev. B **64**, 184523 (2001).

[52] A. Barone and G. Paterno, *Physics and Applications of the Josephson Effect* (Wiley, New York, 1982).

[53] S. Sergeenkov, J. Appl. Phys. **78**, 1114 (1995).

[54] S. Sergeenkov and V.V. Gridin, Phys. Rev. B **50**, 1293 (1994).

[55] V.S. Boiko and A.M. Kosevich, Sov. J. Low. Temp. Phys. **15**, 514 (1989).

[56] Y. Boiko, Materials Lett. **11**, 207 (1991).

[57] R.L. Peterson and J.W. Ekin, Phys. Rev. B **37**, 9848 (1988).

[58] L.D. Landau and E.M. Lifshitz, *Theory of Elasticity* (Pergamon Press, New York, 1960).

[59] M. McElfresh, T.G. Miller, D.M. Schaefer, R. Reifenberger, R.E. Muenchausen, M. Hawley, S.R. Foltyn, and X.D. Wu, J. Appl. Phys. **71**, 5099 (1992).

[60] D.G. Schlom, D. Anselmetti, J.G. Bednorz, R.F. Broom, A. Catana, T. Frey, Ch. Gerber, H.-J. Guntherodt, H.P. Lang, and J. Mannhart, Z. Phys. B **86**, 163 (1992).

[61] J. Mannhart, Mod. Phys. Lett. B **6**, 555 (1992).

[62] R.W. Whitworth, Adv. Phys. **24**, 203 (1975).

[63] Yu. Osipyan, V.F. Petrenko, A.V. Zaretskij, and R.W. Whitworth, Adv. Phys. **35**, 115 (1986).

[64] J.D. Eshelby, Phil. Mag. **3**, 75 (1958).

[65] Z. Tribula, J. Stankowski, and J. Baszynski, Physica C **156**, 485 (1988).

[66] S. Sergeenkov, J. Appl. Phys. **77**, 4831 (1995).

[67] T.S. Orlova and B.I. Smirnov, Supercond. Sci. Technol. **7**, 899 (1994).

[68] T.S. Orlova, B.I. Smirnov, J.Y. Laval, and Yu.P. Stepanov, Supercond. Sci. Technol. **12**, 356 (1999).

[69] A.L. Rakhmanov and A.V. Rozhkov, Physica C **267**, 233 (1996).

[70] D. Dominguez, C. Wiecko, and J.V. José, Phys. Rev. Lett. **83**, 4164 (1999).

[71] J. Mannhart, Supercond. Sci. Technol. **9**, 49 (1996).

[72] S. Sergeenkov and J.V. José, Europhys. Lett. **43**, 469 (1998).

[73] S. Sergeenkov, JETP Lett. **76**, 170 (2002).

[74] L.A. Girifalco, *Statistical Physics of Materials* (A Wiley-Interscience Publication, New York, 1973).

[75] S. Sergeenkov, J. Superconduct. **4**, 431 (1991).

[76] S. Sergeenkov, Physica C **185-189**, 1527 (1991).

[77] S. Sergeenkov, in *Physics and Materials Science of High Temperature Superconductors-II*, vol.**209E**, edited by. R. Kossowsky et al., NATO Advanced Studies Institute Series (Kluwer Academic, Dordrecht, The Netherlands, 1992), pp.125–138.

[78] A. Gurevich and E.A. Pashitskii, Phys. Rev. B **56**, 6213 (1997).

[79] B.H. Moeckly, D.K. Lathrop, and R.A. Buhrman, Phys. Rev. B **47**, 400 (1992).

[80] S. Sergeenkov, Solid State Commun. **79**, 863 (1991).

[81] P. Pureur and J. Schaf, Solid State Commun. **78**, 723 (1991).

[82] S. Sergeenkov, JETP Lett. **77**, 94 (2003).

[83] Jin Xin, Cryogenics **30**, 882 (1990).

[84] B.D. Weaver, M.E. Reeves, G.P. Summers, R.J. Soulen, W.L. Olson, M.M. Eddy, T.W. James, and E.J. Smith, Appl. Phys. Lett. **59**, 2600 (1991).

[85] E.M. Jackson, B.D. Weaver, and G.P. Summers, Appl. Phys. Lett. **64**, 511 (1994).

[86] B.M. Vlcek, H.K. Viswanathan, M.C. Frischherz, S. Fleshler, K. Vandervoort, J. Downey, U. Welp, M.A. Kirk, and G.W. Crabtree, Phys. Rev. B **48**, 4067 (1993).

[87] J.G. Ossandon, J.R. Thompson, Y.C. Kim, Y.R. Sun, D.K. Christen, and B.C. Chakoumakos, Phys. Rev. B **51**, 8551 (1995).

[88] J.G. Ossandon, J.R. Thompson, L. Krusin-Elbaum, H.J. Kim, D.K. Christen, K.J. Song, and J.L. Ullmann, Supercond. Sci. Technol. **14**, 666 (2001).

[89] J.R. Thompson, J.G. Ossandon, L. Krusin-Elbaum, H.J. Kim, K.J. Song, D.K. Christen, and J.L. Ullmann, Advances in Superconductivity **14**, 409 (2002).

[90] K.H. Lee, D. Stroud, and S.M. Girvin, Phys. Rev. B **48**, 1233 (1993).

[91] S. Sergeenkov, in *Studies of High Temperature Superconductors*, vol. **39**, edited by A. Narlikar and F. Araujo-Moreira (Nova Science, New York, 2001), pp. 117–131.

[92] W.A.C. Passos, P.N. Lisboa-Filho, R. Caparroz, C.C. de Faria, P.C. Venturini, F.M. Araujo-Moreira, S. Sergeenkov, and W.A. Ortiz, Physica C **354**, 189 (2001).